10 Salivary Gland Ultrasonography for Primary Sjögren's Syndrome and Juvenile Sjögren's Syndrome

Akaluck Thatayatikom and Sthorn Thatayatikom

10.1 Introduction

Ultrasonography has become widely utilized as a point-of-care diagnostic tool in clinical practice because of its noninvasive and nonirradiating nature, affordable equipment, simple maneuver, high-resolution image, and rescanning at ease in any setting. Anatomical characteristics of major salivary glands (SGs) are well suited to ultrasonography since parotid glands (PGs) and submandibular glands (SMGs) are superficially located with unique echogenicity and vascularity. Understanding normal and abnormal echostructures of major SGs is an essential requirement for salivary gland ultrasonography (SGUS).

The first report of SGUS appeared in the late 1960s [1]. A homogenous pattern and high reflectivity related to multiple, evenly distributed fibrous septa in the normal SGs were described in 1970 [2]. In the 1980s, a B-mode scanning technique described a heterogeneous finding with tiny liquid-like structures, volumetric atrophy, and decreased echogenicity in primary Sjögren's syndrome (pSS) [3, 4]. Homogeneity distinguished SGUS findings of normal subjects from the adults with pSS reported in the 1990s [5]. Similar sonographic changes in juvenile Sjögren's syndrome (jSS) in pediatric patients were reported [6, 7].

Several semiquantitative scoring systems for diagnosing pSS were developed in the past two decades. Sublingual glands (SLGs), the smallest salivary gland of the three pairs of major SGs, were not included in any scoring system since SLGs are too small and varied in size for a reliable evaluation. The scoring systems' variation with different pathological definitions and inconsistency in interpreting SGUS findings yielded diverse diagnostic accuracy [8, 9]. Recently, normal and abnormal PG and SMG features in pSS were defined and validated [10]. A new standardized semiquantitative score was also developed [11] to overcome the concerns of the variation. Implementing SGUS scoring systems as one of the 2016 ACR/EULAR classification criteria for pSS increased the criteria's sensitivity [12–14].

10.2 Normal Salivary Gland Sonographic Anatomy

10.2.1 Parotid Glands (PGs)

PGs are the largest SGs located in the parotid space. The parotid space formed by the superfi-

A. Thatayatikom (✉)
Division of Pediatric Allergy/Immunology/Rheumatology, Department of Pediatrics, University of Florida Shands Children's Hospital, Gainesville, FL, USA
e-mail: atst@ufl.edu

S. Thatayatikom
Division of Pediatric Allergy, Immunology and Rheumatology, Department of Pediatrics, College of Medicine, University of Florida, Gainesville, FL, USA

S. Cha (ed.), *Sjögren's Syndrome and Oral Health*, https://doi.org/10.1007/978-3-030-72029-2_10

cial layer of the deep cervical fascia occupies the space lying below the external auditory canal and the mastoid process's apex and above the mandible angle. The parotid space is lateral to the parapharyngeal space and the carotid space, medial to the superficial space and the subcutaneous tissue, anterior to the carotid space, superior to the submandibular space, and posterior to the masticator space [15]. The PG fills approximately two-thirds of the parotid space. Other structures in the space are Stenson's duct, intraparotid lymph nodes, external carotid artery, retromandibular vein, facial nerve, and auriculotemporal branches of the mandibular division of the trigeminal nerve. Three structures, including the external carotid artery, retromandibular vein, and facial nerve, run parallel, in which the vein is in the middle.

The PG is anatomically divided by the intraparotid facial nerve into two-thirds or superficial lobe laterally to the nerve and one-third or deep lobe medially. The superficial lobe is the portion that overlies the preauricular region, ramus of the mandible, masseter muscle, and posterior mandibular surface. The gland extends superiorly to the zygomatic arch, inferiorly to the sternocleidomastoid muscle (SCM), and posteriorly to the superior border of SCM and mastoid tip (Fig. 10.1). The deep lobe is a small portion behind and deep to the mandibular ramus and lies within the parapharyngeal space [16]. The average gland dimensions are 5.8 and 3.4 cm in the craniocaudal and ventrodorsal axes [17]. The size of the gland is smaller in children and women. There is a high density of periglandular and intraglandular lymph nodes. The intraglandular lymph nodes are unique because of the parotid's late encapsulation during embryogenesis. Approximately 90% of the nodes are periglandular, located between the glandular tissue and capsule [16]. Most of the intraglandular lymph nodes are mainly situated within the upper and lower poles of the glands.

The normal PG parenchyma appears uniformly echotexture (Fig. 10.1b, d) comparable to normal thyroid parenchyma with a clear demarcation between the gland and the overlying tissue [11]. The parotid appears more echogenic than the surrounding muscles but less echogenic than the mandible ramus or mastoid process. In general, the echogenicity of the parenchyma depends on the amount of intraglandular fatty tissues. The gland in children appears smaller and less echogenic (darker) (Fig. 10.1e, f) than the gland in adults due to less fatty infiltration. The superficial lobe is more accessible to visualize than the deep lobe. Since the mandible and the mastoid process block the ultrasound beam, the deep lobe is partially visualized. During the scanning, the masseter muscle and mandible limit the image anteriorly; and mastoid and SCM limit the image posteriorly. Intraglandular lymph nodes are visualized as small, well-defined, and oval-shaped areas of homogenous, hypoechoic cortex with a visible hyperechoic (fatty) hilum (Fig. 10.2a) and positive Doppler's signal (Fig. 10.2b). The unique hyperechoic hilum differentiates the node from other parotid masses. The intraglandular lymph node's short axis in a normal state is usually less than 5–6 mm. The normal Stenson's duct is not visible, except in slim individuals [11]. The duct becomes visualized if it is obstructed. A Doppler ultrasound quickly identifies the two blood vessels, although in some cases, the vessels are barely visible or not visible because of the high-fat content in the gland. The retromandibular vein is typically visualized as a relatively straight vessel near the center of the parotid parenchymal. The external carotid artery is visualized as a deeper vessel in Fig. 10.1e, f. The intraglandular facial nerve is not visible.

10.2.2 Submandibular Glands (SMGs)

SMGs are the second-largest SG and occupy most of the submandibular space, a potential space corresponding to the submandibular triangle. The space is formed by the superficial layer of the deep cervical fascia and is located deep to the platysma muscle and delineated by the anterior and posterior bellies of the digastric muscle and the mandible. The anterior and floor of the space is the mylohyoid muscle, and the posterior of the space is the hyoglossus muscle. The SMG may connect to the PG since it lies

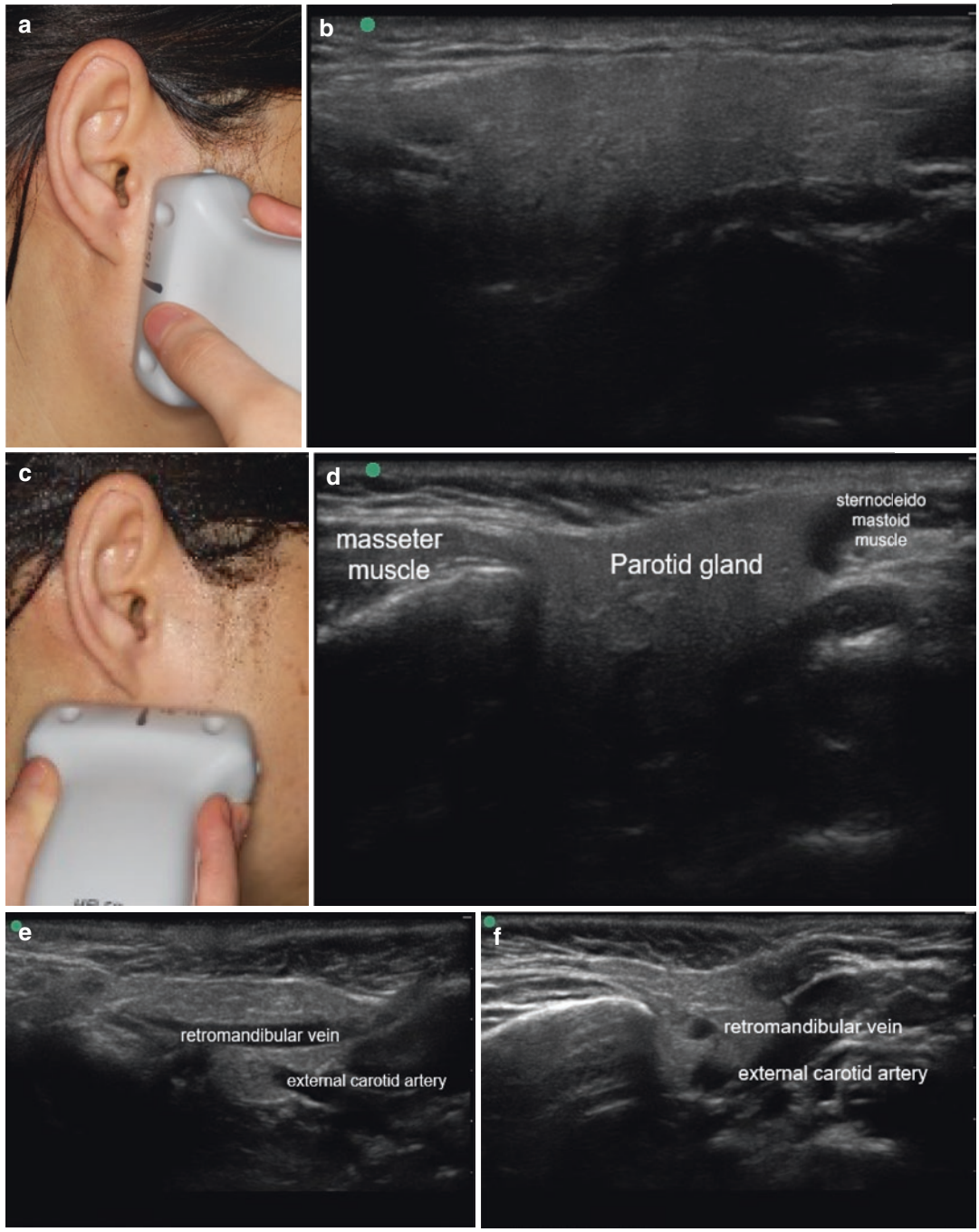

Fig. 10.1 Scanning of the normal parotid gland of a pediatric patient in the longitudinal (**a**, **b**, **e**) and transverse (**c**, **d**, **f**) planes. Children have smaller and slightly darker (less echogenic) gland than adults

anteriorly to the parotid space. The gland is folded around the mylohyoid muscle's dorsal free edge, which divides the gland to be superficial and deep lobes. Submandibular space structures include the superficial lobe of the SMG, submandibular and submental lymph nodes,

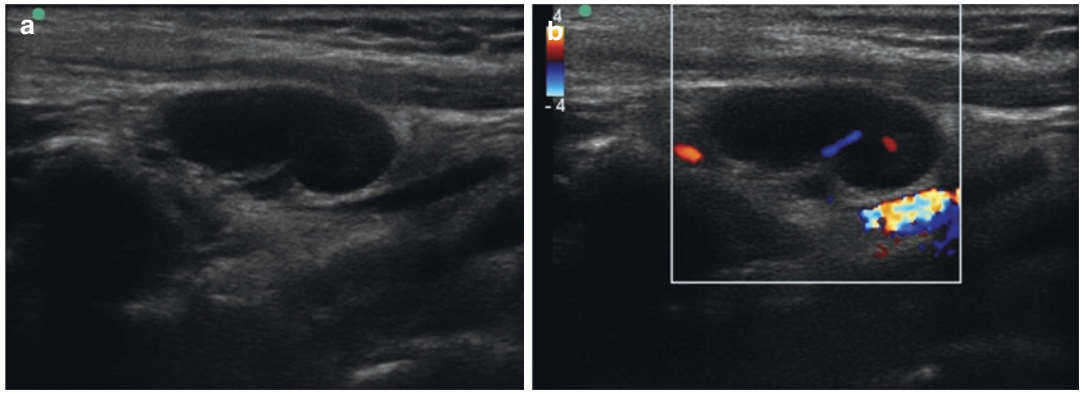

Fig. 10.2 The characteristics of the lymph node with hyperechoic hilum (**a**) and positive color Doppler's signal (**b**) visualized in a pediatric patient

facial artery, facial vein, and hypoglossal nerve's inferior segment. Both facial artery and facial vein are the SMG vessels. The facial artery, the main blood supply, may enter the gland directly. The gland produces approximately 70% of the saliva in the unstimulated state. The Wharton duct, the primary excretory duct, exits the deep lobe's medial surface and drains into the mouth's anterior floor at the sublingual caruncle.

The normal SMG parenchyma appears uniformly echotexture compared with adjacent muscles (Fig. 10.3). SMGs are hypoechoic compared to the PGs and SLGs because of less fatty tissue components. The SMGs look like a triangle in longitudinal (Fig. 10.3b) and transverse (Fig. 10.3d) views. The SMGs in children appear smaller and less echogenic (darker) (Fig. 10.3e, f) than the SMGs in adults due to less fatty infiltration and may connect to the PG (Fig. 10.4a, b). The facial vein is superficial and runs along the anterosuperior part of the gland. The facial artery may cross the SMG's parenchyma in its tortuous course and intersect the gland's posterior pole. Wharton's duct is not visible except in slim individuals. Lymph nodes of SMG are periglandular only.

10.2.3 Sublingual Glands (SLGs)

SLG is the smallest SGs in the sublingual space without a true fascial capsule. The gland lies just deep to the floor of the mouth. The SLG is superior to the mylohyoid muscle and lateral to the genioglossus and geniohyoid muscles, and medial to the mandible. The SLG size shows more significant individual variations than the PGs and SMGs. The gland has no dominant ducts and is drained by ten small ducts (the ducts of Rivinus) into the anterolateral floor of the mouth [18].

The normal SLG parenchyma appears uniformly echotexture with homogeneous hyperechogenicity compared to mylohyoid, genioglossus, and geniohyoid muscles (Fig. 10.5).

10.3 Scanning Technique

1. The patient is in a supine position or upright position. If the supine position is preferred, placing a pillow or towel under the shoulders for neck extension increases thyroid, PGs, and SMGs' accessibility and the patient/operator's comfort.
2. Putting a cotton ball or a 2″ × 2″ nonsterile sponge gauze pad in each ear to protect the ultrasound gel drop into the patient's ear canals.
3. Choosing an available highest-frequency probe such as a 7–14 MHz wideband linear probe. A lower frequency (5–7 MHz) probe may be used to visualize deep portions of the PGs and SMGs.

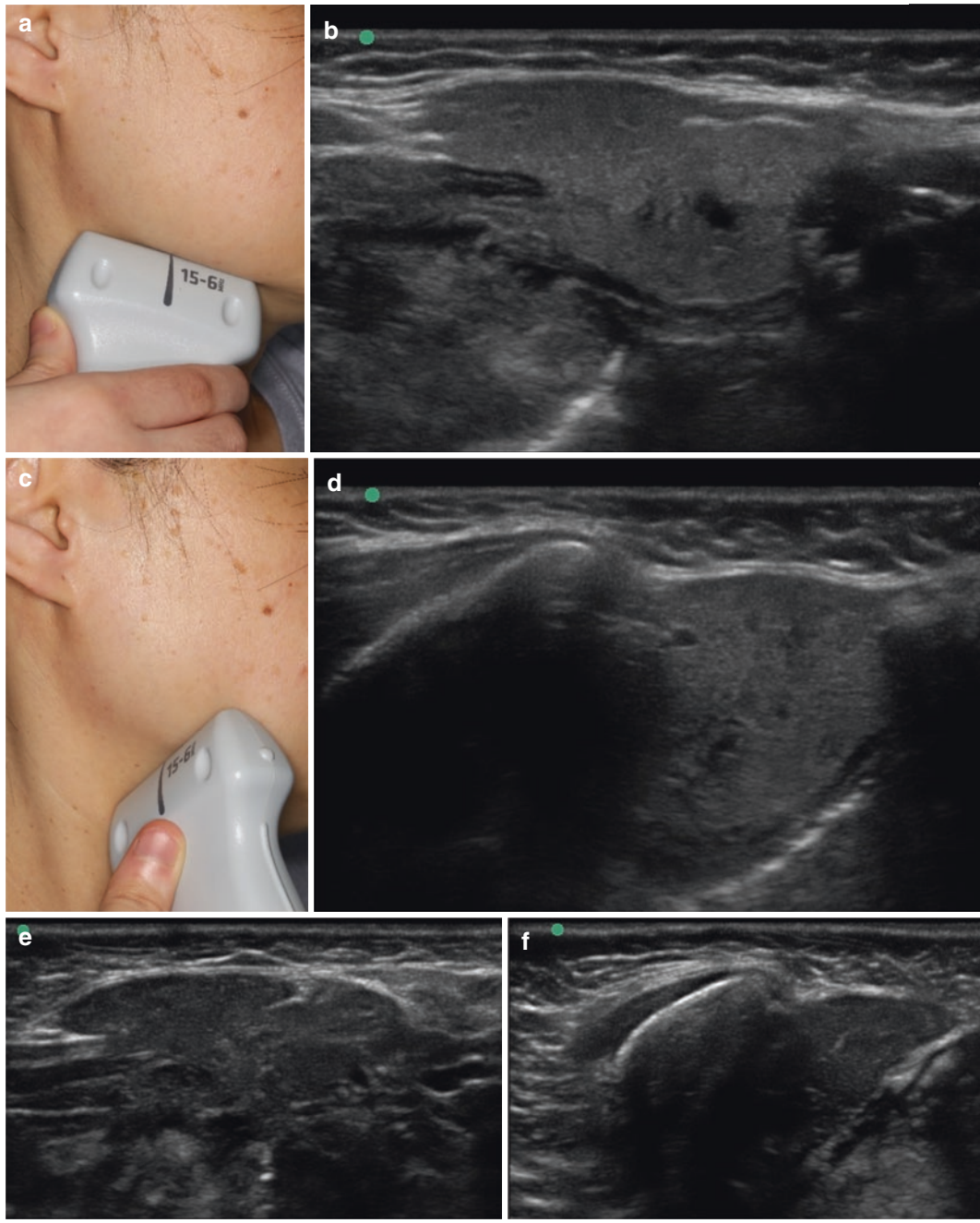

Fig. 10.3 Scanning of the normal submandibular gland of a pediatric patient in the longitudinal (**a**, **b**, **e**) and transverse (**c**, **d**, **f**) planes. Children have smaller and slightly darker (less echogenic) gland than adults

4. Scanning thyroid gland in a longitudinal (Fig. 10.6a, b) and transverse (Fig. 10.6c, d) planes. Thyroid's echogenicity and homogeneity should be reviewed. Inhomogeneous features with anechoic/hypoechoic areas suggest an underlying Hashimoto's thyroiditis (Fig. 10.6e, f).
5. Turning the patient's face away from the examined side when scanning PGs and SMGs. Both PGs and SMGs should be

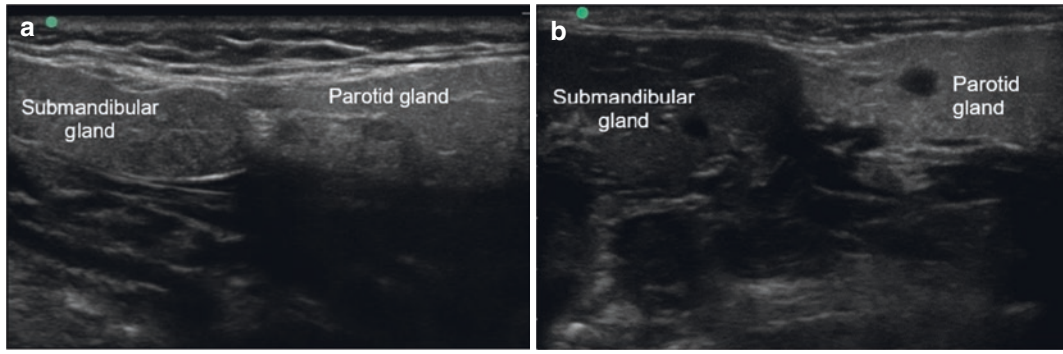

Fig. 10.4 SGUS shows the submandibular gland and parotid gland connection in an adult (**a**) and a 3-year-old boy (**b**). The submandibular glands are less echogenic than the parotid glands, especially in children

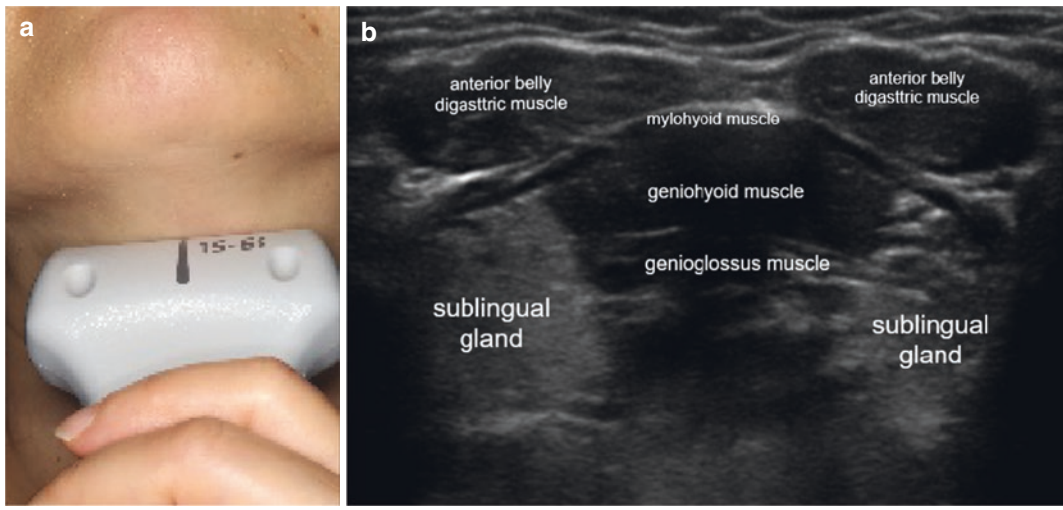

Fig. 10.5 Scanning of the normal sublingual gland of a pediatric patient in the midline transverse plane

scanned in longitudinal and transverse planes and recorded in static images and video clips.

6. Scanning the longitudinal plane of PGs by placing the probe parallel to the mandibular ramus and anterior to the ear (Fig. 10.1a) and scanning the transverse plane of PGs by placing the probe inferior to the ear and perpendicular to the mandible using the mandibular ramus and temporomandibular joint as landmarks (Fig. 10.1c).
7. Scanning the longitudinal plane of SMGs by placing the probe parallel to the mandibular body (Fig. 10.3a) and scanning the transverse plane of SMGs by placing the probe perpendicular to the body of the mandible body (Fig. 10.3c).
8. Scanning vessels and vascularity of PGs and SMGs with color or power Doppler.
9. Assessing echostructures of PGs and SMGs (Table 10.1), including echogenicity, homogeneity, hyperechoic bands, hypoechoic/anechoic areas, fatty replacement, fibrosis, calcifications, lymph nodes, posterior borders, and hypervascularity during the scanning [10].
10. If needed, SLGs can be scanned by placing the probe in the midline transverse or coronal plane of the submental area (Fig. 10.5a).

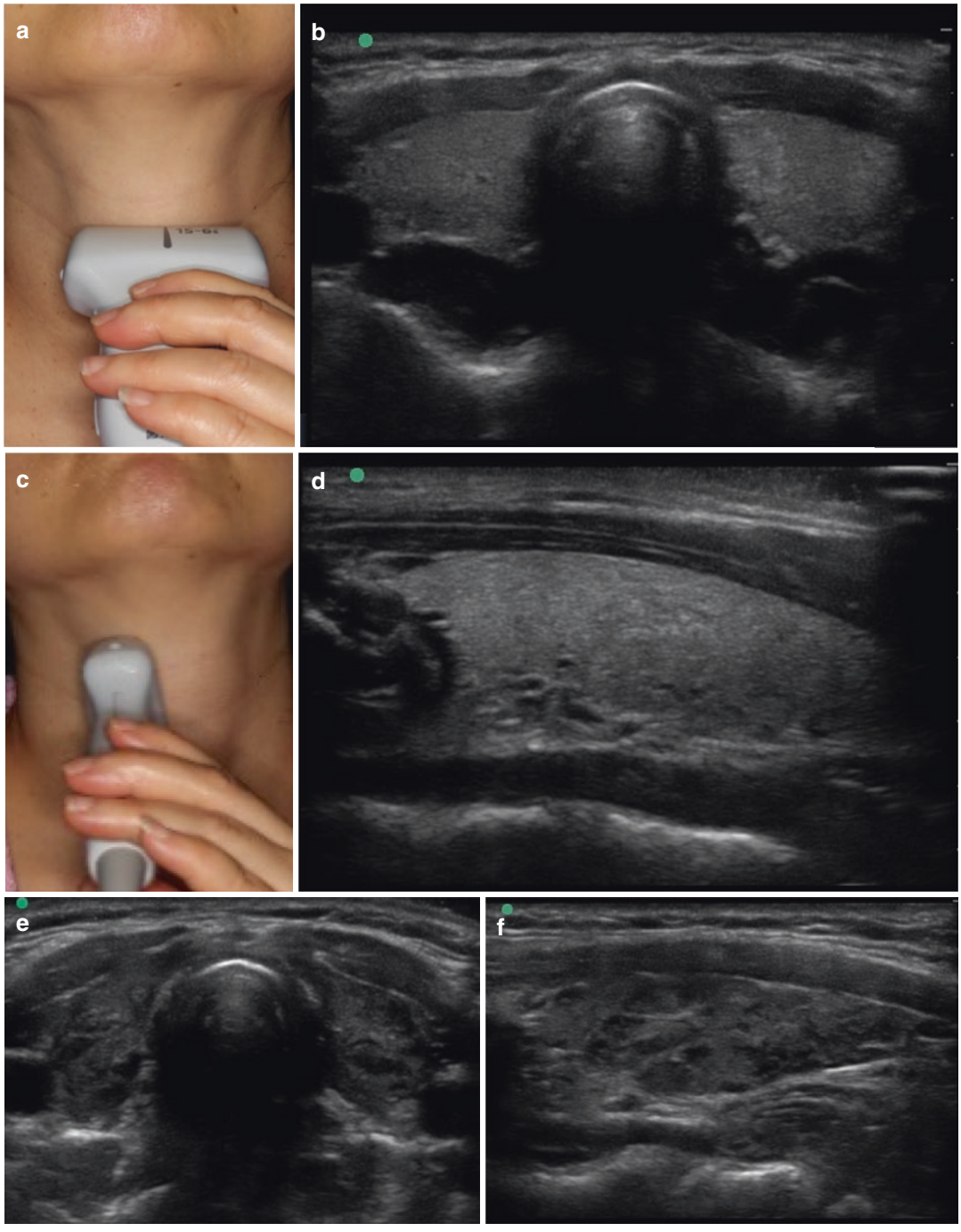

Fig. 10.6 Scanning of the normal thyroid gland of a pediatric patient in the longitudinal (**a**, **b**) and transverse (**c**, **d**) planes. Inhomogeneity with anechoic/hypoechoic findings suggests Hashimoto's thyroiditis (**e**, **f**)

10.4 Abnormal Salivary Gland Ultrasound Findings in Sjögren Syndrome

The essential echostructures in pSS and jSS by B-mode scanning are homogeneity, echogenicity, anechoic/hypoechoic areas. B-mode refers to a two-dimensional ultrasound image display showing bright dots of the ultrasound echoes. Echogenicity and homogeneity are the two SGUS items that determine the intraobserver and interobserver reliability [10]. The homogeneity is strongly correlated with anechoic/hypoechoic areas [11]. Both anechoic/hypoechoic spots and heterogeneous findings (cyst-like heterogeneity) are the most characteristic features for pSS and jSS (Fig. 10.7). The anechoic and hypoechoic areas possibly represent infiltration by lymphocytes, which destroy salivary parenchyma and dilated ducts [19].

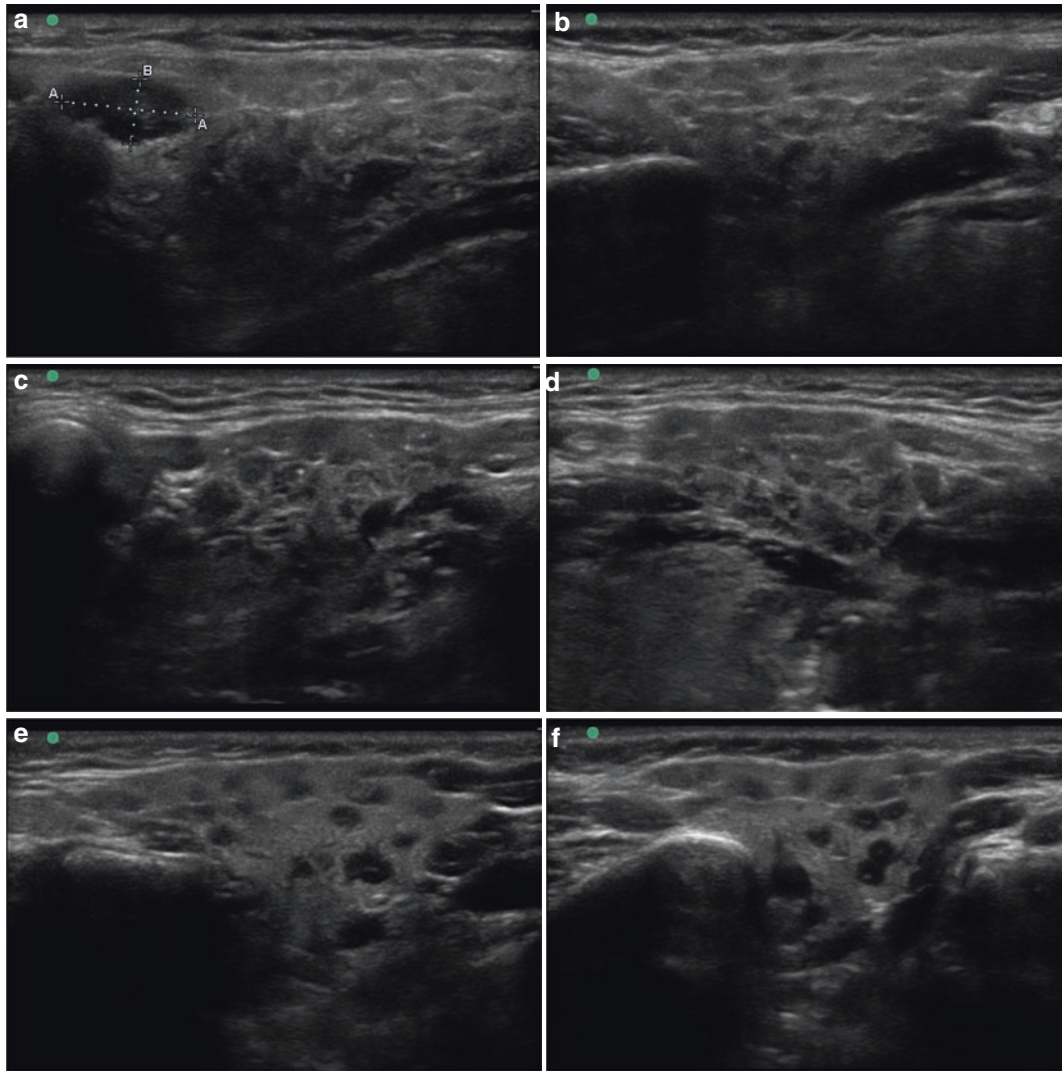

Fig. 10.7 The characteristic SGUS findings of juvenile Sjögren's syndrome. The characteristic heterogeneity and anechoic/hypoechoic areas in parotids (**a**, **b**) and submandibular glands (**c**, **d**) of a teenager boy are shown. Similar findings are found in a 7-year-old girl with juvenile Sjögren's syndrome (**e**, **f**). An enlarged intraglandular lymph node (**a**) and hyperechoic bands (**a**, **b**) are noted

Other SGUS findings (Table 10.1) are hyperechoic foci or intraglandular calcifications, hyperechoic bands, fibrosis, enlarged lymph nodes (Fig. 10.7a), fatty replacement, and changes of the posterior border and the gland size [11, 20, 21]. The hyperechoic calcified foci are typically tiny and do not demonstrate a posterior acoustic shadow. Hypervascularity assessed by color or power Doppler indicates acute flare or SG parenchyma inflammation (Fig. 10.8). The abnormal echostructures do not significantly change within the 2 years of scanning in pSS [22]. The SGUS findings are not pathognomonic for pSS and jSS. Additional clinical information is required to interpret the SGUS abnormalities.

SGUS findings of the right major SG are correlated with the left major SG in pSS. If both PG and SMG scanning cannot be completed, at least one PG and one SMG should be scanned in pSS [23]. It is unknown whether the correlation between the right and left major SG is the same as that of the SGUS findings in jSS. It is possible that the findings of PG are not correlated with those of SMGs since those two types of major SGs glands do not share the same parenchymal echostructure, and the disease severity affecting the glands can vary.

10.5 Salivary Gland Ultrasound Scoring Systems

SGUS has clinically proved its value for the evaluation of pSS and jSS. Various semiquantitative SGUS scoring systems for the diagnosis of pSS were proposed based upon the B-mode scanning.

Table 10.1 Echostructures of parotid and submandibular glands [11, 21]

	Normal	Abnormal
Echogenicity	• Identical to the normal thyroid gland	• Hypoechogenicity: the presence of hypo/anechoic areas • Hyperechogenicity: the presence of fatty infiltration or fibrosis with hyperechoic bands
Homogeneity	• Identical to the normal thyroid gland	• Heterogeneity: the presence of hypo/anechoic areas, numerous hyperechoic bands
Anechoic/hypoechoic area	• Not detected	• Anechoic/hypoechoic areas: small areas located anywhere, not compressible, no blood flow detected by color Doppler, not hyperechoic in the center
Fatty replacement	• Homogenously hyperechoic parenchyma compared with adjacent tissue in healthy elderly individuals	• Fatty replacement is detected in a small group of pSS
Fibrosis	• Not detected except for mild hyperechoic bands	• Hyperechoic bands develop into fibrotic tissue indistinguishable from adjacent soft tissue in early-stage SS and end-stage SS
Lymph nodes	• An anechoic, round, or oval area, less than 1 cm in diameter with or without an echogenic hilus and with or without blood flow by color Doppler • Intraglandular lymph nodes located in the upper and lower poles or the middle of the PG's superficial portion • Intraglandular lymph node not present in SMGs	• Lymph nodes with a diameter greater than 1 cm
Calcifications	• Not detected	• Calcifications: hyperechoic structures with or without acoustic shadowing, located in the parenchyma or ducts
Posterior border	• The posterior border or the deep gland boundary visualized and identified by a hyperechoic line between and adjacent tissues on the transverse and longitudinal views	

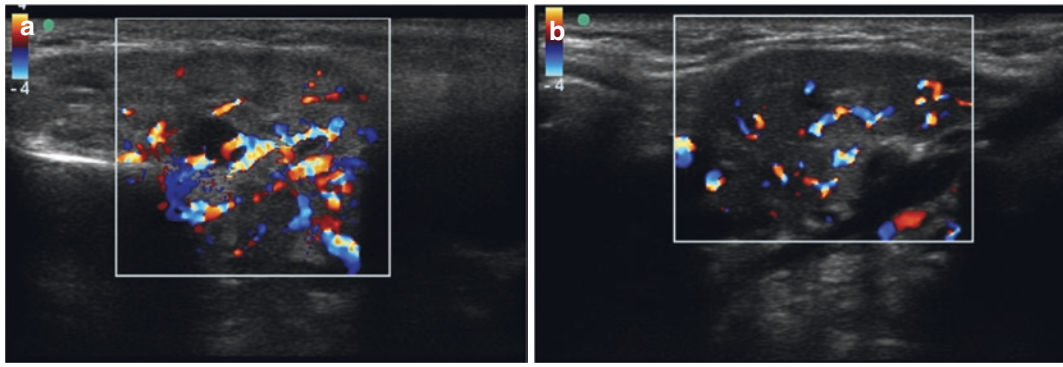

Fig. 10.8 Hypervascularity of active inflammation of the parotid gland (**a**) and submandibular gland (**b**) assessed by color Doppler

The two most reliable and consistent scanning results, echogenicity and homogeneity, are incorporated in most scoring systems. Hyperechoic bands, calcifications, glandular borders, and lymph nodes are unreliable and difficult to assess; however, these findings are applied to certain scoring systems [11, 21].

The first semiquantitative scoring system of SGUS was developed in 1992 [24]. Over 20 scoring systems were subsequently developed in the past two decades. The scoring systems are classified into three systems based upon their total scores: 0–4, 0–16, and 0–48. The Hocevar 0–48 scoring system is the most comprehensive and was applied to several pSS studies [25]. The 0–4 scoring systems show higher specificity and less heterogeneity than others. The 0–4 scoring system is recommended as a universal diagnostic standard [9].

10.5.1 Salivary Gland Ultrasound Scoring System and the Diagnosis of pSS/jSS

A meta-analysis of SGUS scoring systems in diagnosing pSS showed a pooled sensitivity of 69% and specificity of 92% [8]. A negative SGUS result does not exclude a diagnosis of pSS. Table 10.2 shows a few scoring systems with details and the cutoff. Implementing the scoring systems into the 2016 ACR/EULAR classification criteria for the diagnosis of pSS increases the criteria's sensitivity without changing its specificity (Table 10.3). Recently, a novel, reliable, semiquantitative scoring system of SGUS was developed as a consensual scoring system [11]. The usefulness of the novel scoring system in diagnosing pSS and jSS requires further studies.

10.5.2 Salivary Gland Ultrasound Scoring System and Salivary Gland Biopsy

Abnormal SGUS is correlated with minor salivary gland biopsy (MSGB) and PG biopsies in pSS [26–30]. Although a positive SGUS is highly predictive of positive biopsies, they are not interchangeable. The SGUS result cannot replace MSGB in the criteria. Approximately, 16 and 22% of positive SGUS have negative MSGB and PG biopsies, and 26 and 14% of negative SGUS have positive MSGB and PG biopsies accordingly [31]. MSGB remains necessary to perform if SGUS is negative. If SGUS replaces MSGB in the 2016 ACR/ EULAR classification criteria, the criteria's sensitivity is substantially reduced.

10.5.3 Salivary Gland Ultrasound Scoring System and Autoantibodies

Abnormal SGUS may predict SS antibodies' positivity in pSS because of the good agreement of the SGUS and SS antibody results [7, 27, 31–

Table 10.2 Semiquantitative salivary gland ultrasound scoring systems

Authors			
Hocevar [25]	Cornec [61]	Theander [62]	Jousse-Joulin [11]
Score = 0 (each item) • Echogenicity comparable to thyroid • Normal homogeneous • No hypoechogenic area • No hyperechogenic reflections[a] • Clearly defined border of MSG	**Grade = 0** • Normal homogeneous glands	**Score = 0** • Completely homogeneous	**Grade = 0** • Normal parenchyma
Score = 1 (each item) • Decreased echogenicity • Mild inhomogeneity • A few hypoechogenic areas • A few hyperechogenic reflections[a] • Partly defined borders	**Grade = 1** • Small hypoechogenic areas measuring <2 mm with echogenic bands	**Score = 1** • Mildly inhomogeneous	**Grade = 1** • Mild inhomogeneity without anechoic/hypoechoic areas • Diffuse homogeneity with a hyperechoic gland compared with adjacent tissue (fatty echostructure)
Score = 2 (each item) • Inhomogeneity • Several hypoechogenic areas • Several hyperechogenic reflections[a] • Ill-defined borders	**Grade = 2** • Multiple hypoechogenic areas measuring <2 mm with echogenic bands	**Score = 2** • Several rounded hypoechoic lesions	**Grade = 2** • Moderate inhomogeneity with focal anechoic/hypoechoic areas surrounded by normal tissue
Score = 3 (each item) • Grossly inhomogeneous gland • Numerous hypoechogenic areas • Numerous hyperechogenic reflections[a] • Border not visible	**Grade = 3** • Multiple hypoechogenic areas measuring 2–6 mm with hyperechogenic bands	**Score = 3** • Numerous or confluent rounded hypoechoic lesions	**Grade = 3** • Diffuse inhomogeneity with anechoic/hypoechoic areas occupying the entire gland, no normal tissue • Hyperechoic bands of fibrotic tissue indistinguishable from the adjacent soft tissues
NA	**Grade = 4** • Multiple hypoechogenic areas measuring >6 mm • Multiple calcifications with echogenic bands	NA	NA
58.8%[b] 98.7%[c]	62.8%[b] 95%[c]	52%[b] 98%[c]	NA
The cutoff score = 17 (The summation of the scores from the 4 MSGs is calculated)	The cutoff grade = 2 or more (The highest grade of the 4 MSGs is applied)	The cutoff score = 2 or more (The highest score of the 4 MSGs is applied)	NA

[a]The scores are only applied for the parotid glands. The scores of the hyperechogenic reflections of the submandibular glands are 0 (absent) and 1 (present)
[b]Sensitivity
[c]Specificity of SGUS findings of the scoring system

33]. The majority of cases with positive SGUS and anti-SSA fulfill the 2016 ACR/EULAR classification criteria [7, 31]. However, more studies are needed to support whether the combination of the positive SGUS and anti-SSA can replace the MSGB result. More studies of the positive SGUS and anti-SSA are needed to support the findings.

10.5.4 Salivary Gland Ultrasound Scoring System and Sialometry

Abnormal SGUS show an inversed correlation with unstimulated whole salivary flow studies [7, 26–28, 30]. However, the accuracy of abnormal

Table 10.3 Incorporation of salivary gland ultrasonography into the 2016 ACR/EULAR classification criteria

	Items of grayscale (score)	
Author	van Nimwegen [63]	Jousse-Joulin [13]
Grade 0	No hypoechogenic area (0)	No anechoic/hypoechoic area (0)
Grade 1	A few scattered hypoechogenic areas (1)	Hypoechoic areas occupying less than 25% of the gland surface areas (1)
Grade 2	Several hypoechogenic areas (2)	Anechoic/hypoechoic areas occupying 25%–50% of the gland surface areas (2)
Grade 3	Numerous hypoechogenic areas (3)	Anechoic/hypoechoic areas occupying more than 50% of the gland surface areas (3)
Grade 4	NA	Anechoic/hypoechoic areas occupying the entire gland (4)
Sensitivity Specificity	97.3%[a] 90.2%[a]	95.6%[a] 82.6%[a]
Final score and the cutoff	• The average score for hypoechogenic areas of one PG and one SMG • Cutoff score = 1.5 or more for pSS	• The highest MSG score of anechoic/hypoechoic area • Cutoff score = 2 or more for pSS

[a]The sensitivity and specificity of the 2016 ACR/EULAR classification criteria with the addition of SGUS

SGUS to predict salivary gland dysfunction is known to be poor [31].

10.6 SGUS Mimicking Sjögren's Syndrome

10.6.1 Juvenile Recurrent Parotitis (JRP)

Juvenile recurrent parotitis (JRP) is an unknown cause of recurrent nonobstructive, nonsuppurative parotitis in children with unilateral or bilateral PG swellings. The typical presentation is pain, swelling, redness of skin overlying the gland, and fever (Fig. 10.9a). Chronic recurrent parotitis or chronic sialadenitis in adults with the same clinical and sonographic features is less common [34]. SGUS findings in JRP are multiple anechoic/hypoechoic areas, heterogeneous parenchyma echostructures, and hypervascularization with increased Doppler's signal [35]. The hypoechoic areas in JRP correspond to either sialectasis or lymphocytic infiltration [36]. Both JRP and jSS share the same clinical and PG sonographic findings (Figs. 10.9 and 10.10), especially in young children with parotitis and negative SSA/SSB antibodies. Since JRP does not involve minor SGs and SMGs, the positive MSGB and abnormal SMG ultrasound may distinguish these two conditions. Magnetic resonance imaging (MRI) findings of PGs without fat degeneration and architecture destruction possibly suggest JRP [37].

10.6.2 Mumps

Mumps, a paramyxovirus infection, is characterized by painful and inflamed PGs and constitutional symptoms. Bilateral PG involvement is shown in 70% of cases, PG and SMG involvement is presented in 11% of cases, and isolated SMG involvement is noted in 1–2% of cases. Although 30% of infected cases are asymptomatic, severe complications including orchitis, oophoritis, mastitis, pancreatitis, aseptic meningitis, encephalitis, and deafness were reported. SGUS findings in mump are enlarged SG, homogenous echogenicity, heterogeneously hypoechoic intraglandular lymph nodes, and hypervascularity [35, 38].

10.6.3 Chronic Bacterial Infection

An incomplete resolution of an acute infection caused by *Staphylococcus aureus*, *Streptococcus* spp., anaerobic bacteria, and aerobic and facultative Gram-negative bacilli leads to chronic bacterial infection [39]. SGUS shows multiple oval

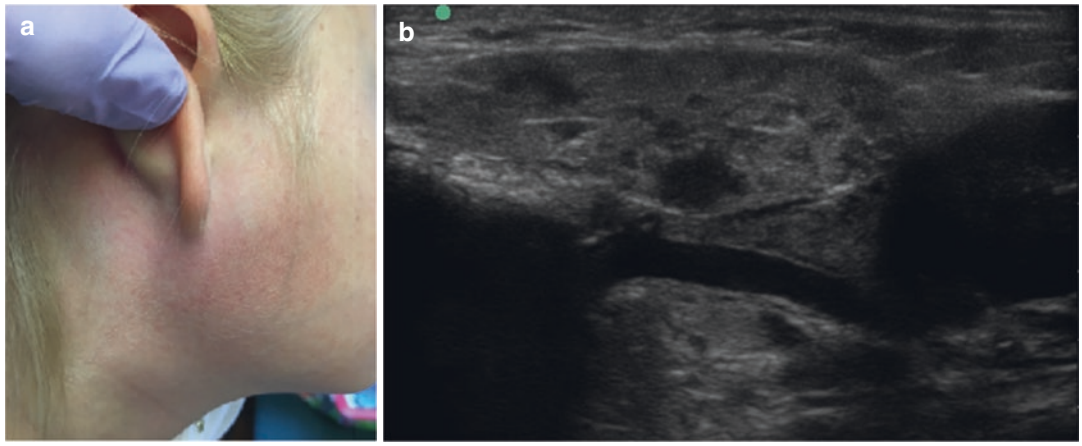

Fig. 10.9 A 6-year-old girl presented with recurrent pain, swelling, and redness of the right parotid gland (**a**) and SGUS revealed heterogeneous parenchyma with multiple anechoic/hypoechoic areas (**b**). Both juvenile Sjögren's syndrome and juvenile recurrent parotitis are common differential diagnoses in young children

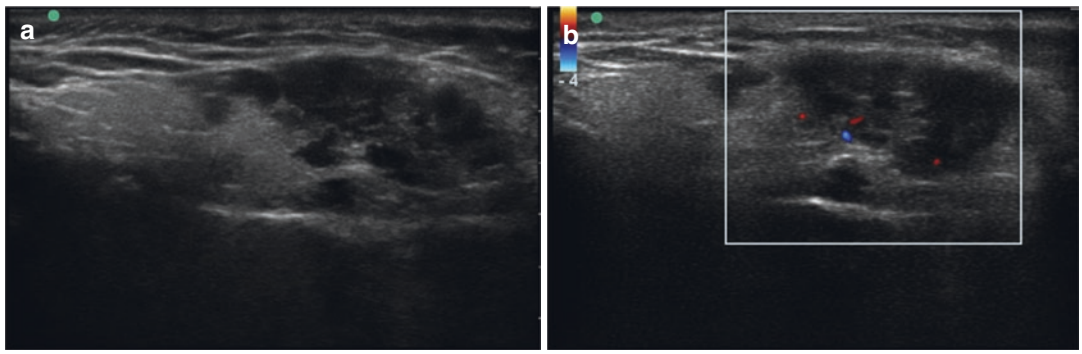

Fig. 10.10 SGUS findings of chronic bacterial infection in a teenager with recurrent pain and swelling of the parotid gland

hypoechoic areas, varying degrees of sialectasis, and hyperechoic septations with hypervascularization (Fig. 10.10) [40].

10.6.4 IgG4-Related Disease

IgG4-related disease (IgG4-RD), a fibroinflammatory disorder, commonly involves SGs [41]. Classic findings of IgG4-RD are bilateral symmetric diffuse swelling of SGs and lacrimal glands. Ultrasonography is considered the most useful imaging modality for IgG4-RD. The characteristic of ultrasound findings in IgG4-RD is a nodal pattern predominantly affecting SMGs (92%) with less-affecting PGs (33%) [42]. The nodal pattern is described as hypoechoic areas with high vascularization and bulging from normal surface commonly detected in SMGs. Both SMGs and PGs are typically homogenous with normal parenchymal echogenicity. The changes are not observed in pSS. The nodal pattern detected by SGUS may not be seen on CT and MRI [43].

10.6.5 Sarcoidosis

Sarcoidosis, a chronic multisystem inflammatory granulomatous disease with unknown etiology, affecting the SGs, involves mostly PGs. Both sarcoidosis and pSS may have similar signs and

symptoms with persistent asymptomatic or painful PG swelling. SGUS findings of sarcoidosis are multiple hypoechoic areas and numerous echogenic septa with the hypervascular area and heterogeneous parenchyma with or without enlarged intraglandular lymph nodes [44]. The findings in sarcoidosis cannot distinguish from the findings in pSS [45].

10.6.6 Systemic Immunoglobulin Light-Chain Amyloidosis (AL Amyloidosis)

AL amyloidosis is the most common form of systemic amyloidosis characterized by the proliferation of clonal plasma cells and immunoglobulin light-chain production, leading to SG enlargement and other organ damage [46]. SGUS findings in AL amyloidosis are hypoechoic lesions and hyperechoic septa, similar to the findings in pSS [45].

10.6.7 HIV Infections

HIV-associated SG disease commonly involves bilateral PGs. Typically, the parotitis is asymmetrical, painless, slow-growing with xerostomia, and salivary gland hypofunction. The PG ultrasound findings in HIV-infected patients can be normal and abnormal. There are four distinct ultrasound patterns including (1) lymphocytic aggregations (diffuse small hypoechoic or anechoic areas with moderate to ill-defined margins interspersed within normal isoechoic areas, not associated with posterior acoustic enhancement), (2) lymphoepithelial cysts, a pathognomonic of HIV infection (well-circumscribed round hypoechoic area with size 5 mm or larger and posterior acoustic enhancement), (3) fatty infiltration (whole hypoechoic gland), and (4) lymphadenopathy (oval-shaped hypoechoic areas or nodules with echogenic hilum and hilar blood flow). Both lymphocytic aggregations and lymphoepithelial cysts may be similar to the findings in SS [47].

10.6.8 Lymphoma

Lymphomas are the second most common malignancies in the head and neck. SG lymphomas can be primary or secondary, and extranodal (arising outside a lymphoid organ) or nodal (appearing inside an intraglandular lymph node or periparotid lymph node) [48]. Primary SG lymphomas commonly involve unilateral or bilateral PGs, and most are classified as extranodal marginal-zone B-cell non-Hodgkin's lymphoma originating from mucosa-associated lymphoid tissue (MALT) [49]. SS is a well-known risk factor for primary SG lymphoma. There are two defined sonographic patterns of SG lymphomas, including linear echogenic strands pattern and segmental pattern. The linear echogenic strands pattern is a marked hypoechoic area with interspersed linear echogenic strands, and the segmental pattern is multiple, relatively large hypoechoic segments. The SGUS findings represent the histopathologic findings of expanding lymphoma cells demarcated by narrow or wide fibrous bands [50, 51].

10.6.9 Postradiotherapy

Radiotherapy alters and damages PG parenchyma and SG acinar cells leading to xerostomia. SGUS of PG postradiotherapy appears isoechoic or hypoechoic echogenicity, small gland size, heterogeneous echotexture with multiple hypoechoic areas, and hyperechoic fibrotic streaks [52].

10.7 Other Imaging for Primary Sjögren's Syndrome and Juvenile Sjögren's Syndrome

10.7.1 Plain Radiograph

A plain radiograph is an inexpensive and simple study for evaluating salivary stones, especially SMG stones since the SMG stones are relatively large and radiopaque [53]. It has no diagnostic role for pSS and jSS.

10.7.2 Sialography

Sialography is an old diagnostic procedure based on the injection of a dye into the salivary duct orifice (Stenson and Wharton duct) to visualize the entire ductal architecture and identify salivary calculi, ductal anomaly, and stricture. Abnormal sialography with diffuse sialectasis, including punctate, cavity, or destructive pattern, is a criterion in the 2002 American-European Consensus Group (AECG) classification. The abnormal findings result from cystic ductal dilatations or extravasation of the contrast material into the parenchyma. The extravasation of the contrast material is possibly related to the dysfunction of tight junctions between striated ductal cells caused by inflammatory cytokines. Its sensitivity and specificity are 80 and 89% based upon the 2002 AECG criteria [54].

Sialography is excluded from the 2016 ACR/EULAR criteria because of its invasiveness, potential complications including ductal rupture or activation of dormant infection, irradiating nature, and contraindications such as acute infection, acute inflammation, and contrast allergy. SGUS has replaced sialography since it provides similar information while being considerably less invasive.

10.7.3 Salivary Gland Scintigraphy

Salivary gland scintigraphy, a nuclear imaging technique with radioactive tracer infusion (Technetium-99m pertechnetate), demonstrates the glandular function by evaluating the distribution and speed of eliminating the radiotracer after a secretive stimulation. It reveals both physiologic and pathologic secretory functions. The potential benefit of scintigraphy is to monitor SG functioning over time.

Abnormal scintigraphy results are delayed uptake, reduced concentration, and delayed excretion of tracer described in the 2002 AECG criteria. Its sensitivity and specificity are 89 and 50% [55]. Although it is noninvasive, safe, well-tolerated, reproducible, and easy to perform, the test results cannot distinguish the secretive dysfunction of pSS from other diseases [55]. In addition, there are no guidelines or consensus on how the test should be performed and interpreted [56].

10.7.4 Computed Tomography (CT)

Computed tomography (CT) and MRI identify the homogeneity and inhomogeneity of adipose tissue distribution and accumulation related to destruction and shrinkage from chronic inflammation. CT is more readily available and lower-cost with a shorter scan time than MRI. Non-contrast-enhanced CT is useful in identifying small calculi in the gland or duct. Contrast-enhanced CT is useful where MRI is contraindicated, or the access to MRI is limited.

Normal fatty tissue inside the PGs is homogeneously distributed and contributes to the low CT attenuation regardless of the subject's age. Abnormal CT findings of the PGs in SS include heterogeneity of attenuation caused by fatty degeneration, abnormal fat tissue deposition, diffuse punctate calcification, atrophy or swelling of the gland, nodularity, and cystic lesions. The diffuse punctate calcification of bilateral PGs is highly specific for SS and found in 30% of cases [57]. The drawback of CT scan is radiation exposure, artifacts from metal dental fillings, and its contraindications, including impaired kidney function and contrast hypersensitivity.

10.7.5 Magnetic Resonance Imaging (MRI) and Magnetic Resonance Sialography (MR Sialography)

MRI is noninvasive, nonionizing imaging, providing pathologic changes of major SG in SS. T1-weighted image and fat-suppressed T2-weighted image are recommended. Intravenous injection of a contrast medium increases the detection of abnormalities, but it is not mandatory for SS diagnosis. Normal PGs are intermediate to high single intensity on T1- and T2-weighted images due to high intraglandular fat content. The submandibular and sublingual

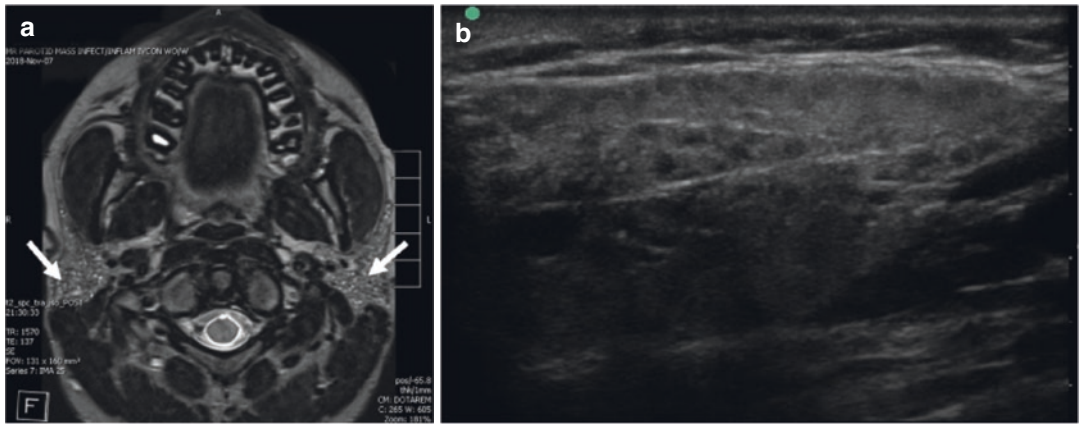

Fig. 10.11 A characteristic MRI finding of the parotid gland of a teenager with juvenile Sjögren's syndrome shows salt-and-pepper appearance (**a**, white arrow) compared to SGUS (**b**)

glands demonstrate a more intermediate signal on T1-weighted image [58]. MRI can identify early SS with edema and gland enlargement, lobular destruction with diffuse micro and/or macrocystis changes associated with deposition of fibrous tissue and fat [55]. Both high-signal intensity on T1- and T2-weighted images and low-signal intensity in fat-suppressed T2-weighted images indicate abnormal adipose tissue deposition. The characteristic MRI of PGs and SMGs is heterogeneous signal intensity (mixed low- and high-signal intensity) distribution on T1- and T2-weighted images with a salt-and-pepper appearance or a honeycomb appearance (Fig. 10.11).

MR sialography, a new modification of MRI, reveals early diseases of PG without the injection of contrast material. MR sialography is obtained with a heavily T2-weighted 3D-Fast spin-echo appearance. MR sialography's abnormal findings are multiple high-signal-intensity spots with apple tree appearance and enlargement or reduction of the gland's size. A combination of MRI and MR sialography provides high sensitivity and specificity for observing parenchymal abnormalities and differentiation of SS [59, 60].

The significant disadvantages of MRI and MR sialography are higher cost, length of the examination, patient intolerance, sedation requirement in young children, and its contraindications, including retained metallic foreign bodies such as dental braces, cardiac pacemakers, or insulin pumps.

10.8 Conclusion

SGUS has been increasingly used as a first-line imaging tool to evaluate and diagnose pSS and jSS with reasonable accuracy. It offers a noninvasive assessment of typical morphological changes in the major SGs. There is growing evidence to support the abnormal sonographic features as a criterion for the next disease classification. The potential roles of SGUS in reducing the need for MSGB and monitoring treatment response require further studies.

References

1. Kitamura T, et al. Ultrasonic diagnosis in oto-rhinolaryngology. Eye Ear Nose Throat Mon. 1969;48(5):329–37.
2. Baker S, Ossoinig KC. Ultrasonic evaluation of salivary glands. Trans Sect Otolaryngol Am Acad Ophthalmol Otolaryngol. 1977;84(4 Pt 1):Orl-750-62.
3. de Clerck LS, et al. Ultrasonography and computer tomography of the salivary glands in the evaluation of Sjögren's syndrome. Comparison with parotid sialography. J Rheumatol. 1988;15(12):1777–81.
4. Bruneton JN, et al. Indications for ultrasonography in parotid pathologies. Rofo. 1983;138(1):22–4.

5. Kawamura H, et al. Salivary gland echography in patients with Sjögren's syndrome. Arthritis Rheum. 1990;33(4):505–10.
6. Civilibal M, et al. A child with primary Sjogren syndrome and a review of the literature. Clin Pediatr (Phila). 2007;46(8):738–42.
7. Hammenfors DS, et al. Juvenile Sjögren's syndrome: clinical characteristics with focus on salivary gland ultrasonography. Arthritis Care Res (Hoboken). 2020;72(1):78–87.
8. Delli K, et al. Diagnostic properties of ultrasound of major salivary glands in Sjogren's syndrome: a meta-analysis. Oral Dis. 2015;21(6):792–800.
9. Zhou M, et al. Diagnostic accuracy of salivary gland ultrasonography with different scoring systems in Sjogren's syndrome: a systematic review and meta-analysis. Sci Rep. 2018;8(1):17128.
10. Jousse-Joulin S, et al. Salivary gland ultrasound abnormalities in primary Sjogren's syndrome: consensual US-SG core items definition and reliability. RMD Open. 2017;3(1):e000364.
11. Jousse-Joulin S, et al. Video clip assessment of a salivary gland ultrasound scoring system in Sjogren's syndrome using consensual definitions: an OMERACT Ultrasound Working Group reliability exercise. Ann Rheum Dis. 2019;78:967–73.
12. Geng Y, et al. Salivary gland ultrasound integrated with 2016 ACR/EULAR classification criteria improves the diagnosis of primary Sjogren's syndrome. Clin Exp Rheumatol. 2020;38(2):322–8.
13. Jousse-Joulin S, et al. Weight of salivary gland ultrasonography compared to other items of the 2016 ACR/EULAR classification criteria for primary Sjogren's syndrome. J Intern Med. 2020;287(2):180–8.
14. van Nimwegen JF, et al. Incorporation of salivary gland ultrasonography into the American College of Rheumatology/European League Against Rheumatism criteria for primary Sjogren's syndrome. Arthritis Care Res (Hoboken). 2020;72(4):583–90.
15. Gervasio A, et al. Sonographic anatomy of the neck: the suprahyoid region. J Ultrasound. 2011;14(3):130–5.
16. Kochhar A, Larian B, Azizzadeh B. Facial nerve and parotid gland anatomy. Otolaryngol Clin N Am. 2016;49(2):273–84.
17. Silvers AR, Som PM. Salivary glands. Radiol Clin N Am. 1998;36(5):941–66, vi.
18. Abdullah A, Rivas FF, Srinivasan A. Imaging of the salivary glands. Semin Roentgenol. 2013;48(1):65–74.
19. Bialek EJ, et al. US of the major salivary glands: anatomy and spatial relationships, pathologic conditions, and pitfalls. Radiographics. 2006;26(3):745–63.
20. Cornec D, et al. Salivary gland ultrasound to diagnose Sjögren's syndrome: a claim to standardize the procedure. Rheumatology. 2014;54(1):199–200.
21. Jousse-Joulin S, et al. Salivary gland ultrasound abnormalities in primary Sjögren's syndrome: consensual US-SG core items definition and reliability. RMD Open. 2017;3(1):e000364.
22. Gazeau P, et al. Time-course of ultrasound abnormalities of major salivary glands in suspected Sjögren's syndrome. Joint Bone Spine. 2018;85(2):227–32.
23. Mossel E, et al. Scoring hypoechogenic areas in one parotid and one submandibular gland increases feasibility of ultrasound in primary Sjogren's syndrome. Ann Rheum Dis. 2018;77(4):556–62.
24. De Vita S, et al. Salivary gland echography in primary and secondary Sjögren's syndrome. Clin Exp Rheumatol. 1992;10(4):351–6.
25. Hocevar A, et al. Ultrasonographic changes of major salivary glands in primary Sjogren's syndrome. Diagnostic value of a novel scoring system. Rheumatology (Oxford). 2005;44(6):768–72.
26. Baldini C, et al. Salivary gland ultrasonography: a highly specific tool for the early diagnosis of primary Sjogren's syndrome. Arthritis Res Ther. 2015;17:146.
27. Hammenfors DS, et al. Diagnostic utility of major salivary gland ultrasonography in primary Sjogren's syndrome. Clin Exp Rheumatol. 2015;33(1):56–62.
28. Cornec D, et al. High-grade salivary-gland involvement, assessed by histology or ultrasonography, is associated with a poor response to a single rituximab course in primary Sjögren's syndrome: data from the TEARS randomized trial. PLoS One. 2016;11(9):e0162787.
29. Astorri E, et al. Ultrasound of the salivary glands is a strong predictor of labial gland biopsy histopathology in patients with Sicca symptoms. J Oral Pathol Med. 2016;45(6):450–4.
30. Kim JW, et al. Salivary gland ultrasonography findings are associated with clinical, histological, and serologic features of Sjogren's syndrome. Scand J Rheumatol. 2018;47(4):303–10.
31. Mossel E, et al. Ultrasonography of major salivary glands compared with parotid and labial gland biopsy and classification criteria in patients with clinically suspected primary Sjogren's syndrome. Ann Rheum Dis. 2017;76(11):1883–9.
32. Nieto-Gonzalez JC, et al. Salivary gland ultrasound is linked to the autoimmunity profile in patients with primary Sjogren's syndrome. J Int Med Res. 2018;48:300060518767031.
33. Lee KA, Lee SH, Kim HR. Diagnostic and predictive evaluation using salivary gland ultrasonography in primary Sjögren's syndrome. Clin Exp Rheumatol. 2018;36 Suppl 112(3):165–72.
34. Abdel Razek AAK, Mukherji S. Imaging of sialadenitis. Neuroradiol J. 2017;30(3):205–15.
35. Sitheeque M, et al. Juvenile recurrent parotitis: clinical, sialographic and ultrasonographic features. Int J Paediatr Dent. 2007;17(2):98–104.
36. Papadopoulou-Alataki E, et al. Juvenile recurrent parotitis: the role of sialendoscopy. Int J Inflamm. 2019;2019:7278907.
37. Kimura Y, et al. Magnetic resonance imaging-based differentiation between juvenile recurrent parotitis and juvenile Sjögren's syndrome. Oral Radiol. 2011;27(1):73–7.

38. Sirmatel O, et al. Radiological findings in a mumps case with multiple complications. Indian J Radiol Imaging. 2006;16(3):305–8.
39. Brook I. The bacteriology of salivary gland infections. Oral Maxillofac Surg Clin North Am. 2009;21(3):269–74.
40. Orlandi MA, Pistorio V, Guerra PA. Ultrasound in sialadenitis. J Ultrasound. 2013;16(1):3–9.
41. Maritati F, Peyronel F, Vaglio A. IgG4-related disease: a clinical perspective. Rheumatology (Oxford). 2020;59(Suppl 3):iii123–31.
42. James-Goulbourne T, Murugesan V, Kissin EY. Sonographic features of salivary glands in Sjögren's syndrome and its mimics. Curr Rheumatol Rep. 2020;22(8):36.
43. Shimizu M, et al. Effectiveness of imaging modalities for screening IgG4-related dacryoadenitis and sialadenitis (Mikulicz's disease) and for differentiating it from Sjögren's syndrome (SS), with an emphasis on sonography. Arthritis Res Ther. 2015;17(1):223.
44. Teymoortash A, Werner JA. Parotid gland involvement in sarcoidosis: sonographic features. J Clin Ultrasound. 2009;37(9):507–10.
45. Law ST, et al. Comparison of ultrasound features of major salivary glands in sarcoidosis, amyloidosis, and Sjögren's syndrome. Arthritis Care Res (Hoboken). 2020;72(10):1466–73.
46. Merlini G, et al. Systemic immunoglobulin light chain amyloidosis. Nat Rev Dis Primers. 2018;4(1):38.
47. Kabenge C, et al. Diagnostic ultrasound patterns of parotid glands in human immunodeficiency virus-positive patients in Mulago, Uganda. Dentomaxillofac Radiol. 2010;39(7):389–99.
48. Cabeçadas J, et al. Lymphomas of the head and neck region: an update. Virchows Arch. 2019;474(6):649–65.
49. Paliga A, et al. Salivary gland lymphoproliferative disorders: a Canadian tertiary center experience. Head Neck Pathol. 2013;7(4):381–8.
50. Bahn YE, et al. Sonographic appearances of mucosa-associated lymphoid tissue lymphoma of the submandibular gland confirmed with sonographically guided core needle biopsy. J Clin Ultrasound. 2011;39(4):228–32.
51. Orita Y, et al. Characteristic ultrasound features of mucosa-associated lymphoid tissue lymphoma of the salivary and thyroid gland. Acta Otolaryngol. 2014;134(1):93–9.
52. Ying M, Wu VW, Kwong DL. Comparison of sonographic appearance of normal and postradiotherapy parotid glands: a preliminary study. Ultrasound Med Biol. 2007;33(8):1244–50.
53. Bag AK, et al. Imaging of inflammatory disorders of salivary glands. Neuroimaging Clin N Am. 2018;28(2):255–72.
54. Song GG, Lee YH. Diagnostic accuracies of sialography and salivary ultrasonography in Sjogren's syndrome patients: a meta-analysis. Clin Exp Rheumatol. 2014;32(4):516–22.
55. Baldini C, et al. Imaging in primary Sjogren's syndrome: the 'obsolete and the new'. Clin Exp Rheumatol. 2018;36 Suppl 112(3):215–21.
56. Afzelius P, et al. Imaging of the major salivary glands. Clin Physiol Funct Imaging. 2016;36(1):1–10.
57. Sun Z, et al. Diagnostic accuracy of parotid CT for identifying Sjögren's syndrome. Eur J Radiol. 2012;81(10):2702–9.
58. Nayak GK, Hagiwara M. Imaging of salivary gland pathology. Oper Tech Otolaryngol Head Neck Surg. 2018;29(3):116–28.
59. Niemela RK, et al. Magnetic resonance imaging and magnetic resonance sialography of parotid glands in primary Sjogren's syndrome. Arthritis Rheum. 2001;45(6):512–8.
60. Tomiita M, et al. Usefulness of magnetic resonance sialography in patients with juvenile Sjogren's syndrome. Clin Exp Rheumatol. 2005;23(4):540–4.
61. Cornec D, et al. Contribution of salivary gland ultrasonography to the diagnosis of Sjögren's syndrome: toward new diagnostic criteria? Arthritis Rheum. 2013;65(1):216–25.
62. Theander E, Mandl T. Primary Sjogren's syndrome: diagnostic and prognostic value of salivary gland ultrasonography using a simplified scoring system. Arthritis Care Res (Hoboken). 2014;66(7):1102–7.
63. van Nimwegen JF, et al. Incorporation of salivary gland ultrasonography into the American College of Rheumatology/European League Against Rheumatism criteria for primary Sjogren's syndrome. Arthritis Care Res. 2020;72(4):583–90.